Supporting Information

Symmetry Lowering in Triindoles: Impact on the Electronic and Photophysical Properties

Constanza Ruiz, Eva M. Garcia-Frutos, Demetrio A. da Silva Filho, Juan T. López Navarrete,*

M. Carmen Ruiz Delgado* and Berta Gómez-Lor*

*E-mail: bgl@icmm.csic.es, teodomiro@uma.es; carmenrd@uma.es

Supporting Information

1. Characterization of compound 2c

Characterization of 5,6,11-trioctyl-6,11-dihydro-5H-diindolo[2,3-a:2',3'-c]carbazole (**2c**). ^{1}H NMR (200 MHz, $CDCl_3$, δ) δ 8.96 (d, J = 7.9Hz, 1 H; ArH), 8.90 (d, J = 7.7 Hz, 1 H; ArH), 8.41 (d, J = 8.1 Hz, 1 H; ArH), 7.70-7.63 (m; 3H, ArH), 7.57-7.33(m, 6 H; ArH), 4.95 (t, J = 7.9 Hz, 2 H; CH_2), 4.70 (t, J = 7.4 Hz, 2 H; CH_2), 4.58 (t, J = 7.5 Hz, 2 H; CH_2), 2.10 (m, 6 H; CH_2), 1.47-0.82 (m, 30 H; CH_2), 0.71 (m, 9 H; CH_3); ^{13}C NMR (50 MHz, $CDCl_3$, δ) 144.7, 143.3, 140.8, 133.8, 131.8, 127.0, 126.8, 125.2, 124.5, 124.1, 123.9, 123.5, 123.1, 122.7, 122.2, 120.3, 119.6, 119.0, 112.7, 112.5, 112.0, 109.8, 48.5, 48.0, 46.8, 31.7, 31.6, 31.5, 30.4, 29.7, 29.3, 29.2, 28.9, 28.8, 27.4, 27.0, 26.8, 26.6, 26.4, 22.6, 22.5, 14.1, 14.0; UV-vis (CH_2Cl_2, 25 ºC): λ_{max} (ε) = 263 (7447), 309 (7674), 343 (3219), 357 (4092), 390 (1681), 408 (1844) nm; MALDI-TOF MS *m*/*z* 681 [M^+], HRMS (MALDI-TOF) calcd for $C_{48}H_{63}N_3$: 681.50165, found: 681.50189.

2. Absorption spectra

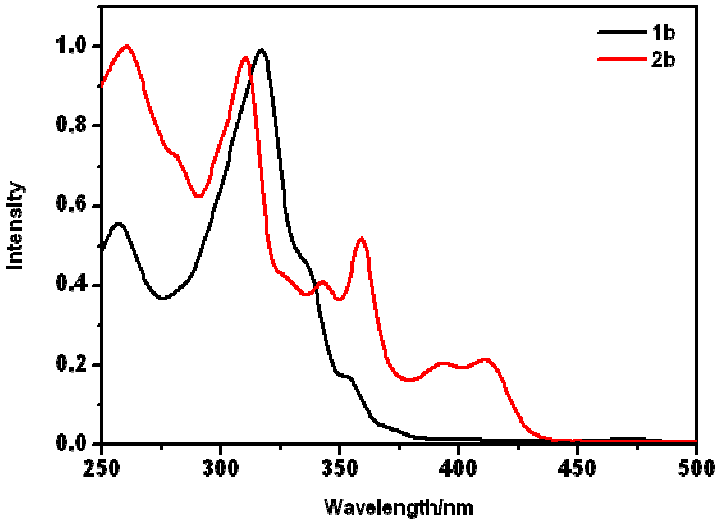

Figure S1. Experimental UV-Vis spectra of **1b** and **2b** in CH_2Cl_2 solutions.

3. Cyclic Voltammetry Measurements

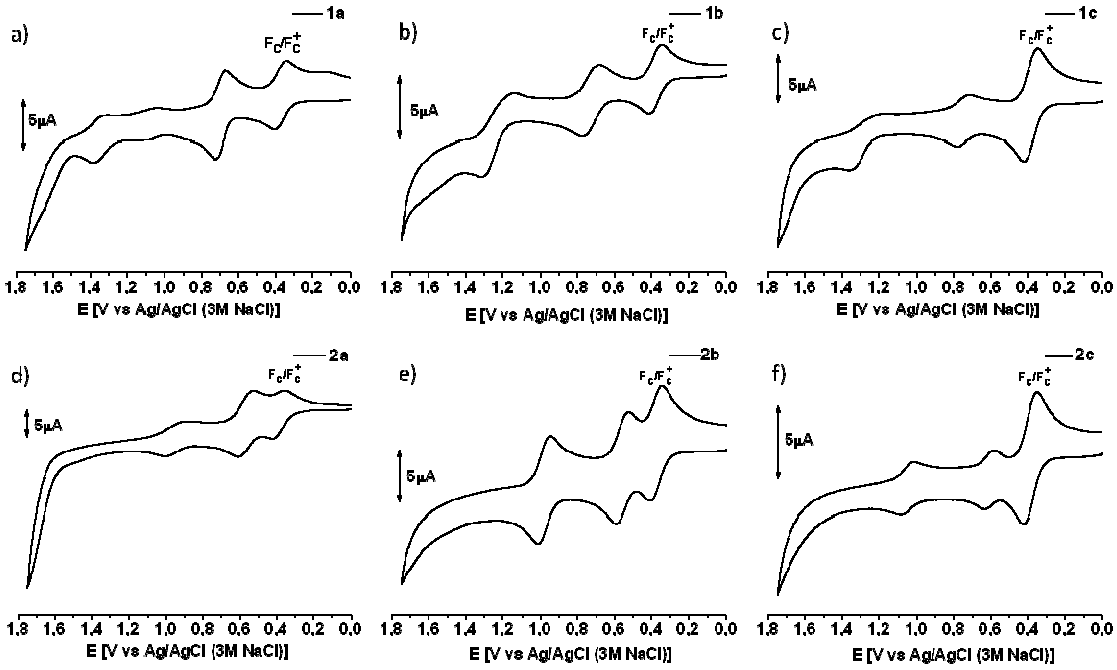

Figure S2. Cyclic voltammograms of **1a**, **1b**, **1c**, **2a**, **2b** and **2c** at c = $1x10^{-3}$ $molL^{-1}$ recorded in CH_3CN/ 0.1M tetra-*n*-butylammonium hexafluorophosphate ($TBAPF_6$) measured versus Ag/AgCl (3M NaCl) and containing ferrocene as internal standard. Measurements were performed at a scan rate 100mV/s using a Pt working electrode and a Pt wire auxiliary electrode.

4. Spectroelectrochemistry and chemical oxidation

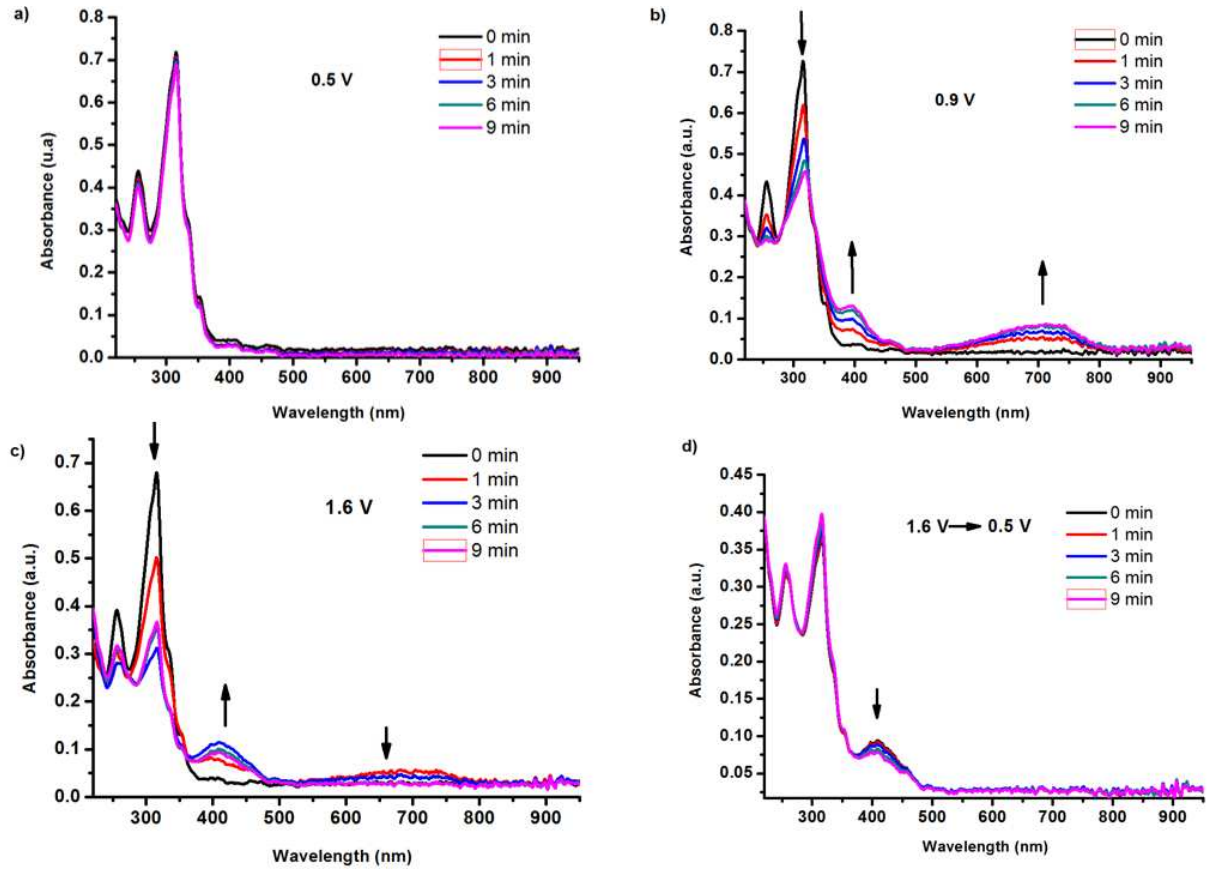

Figure S3: Spectroelectrochemistry of **1c** in acetonitrile solution containing 0.1 M Bu_4NPF_6 as supporting electrolyte at a) 0.5 V, b) 0.9 V c) 1.6 V and d) recovery of the compound from 1.6 to 0.5 V.

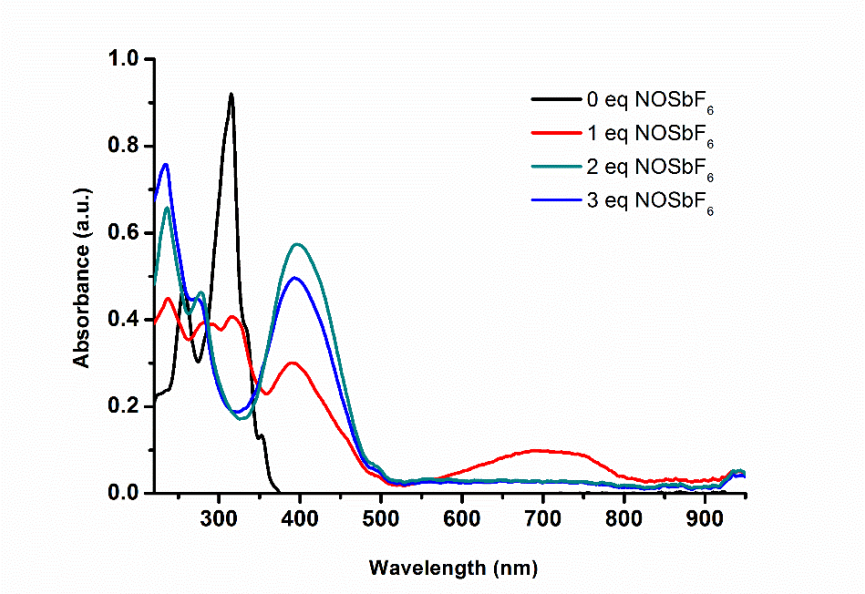

Figure S4: Chemical oxidation of **1c** in acetonitrile with different equivalent of $NOSbF_6$.

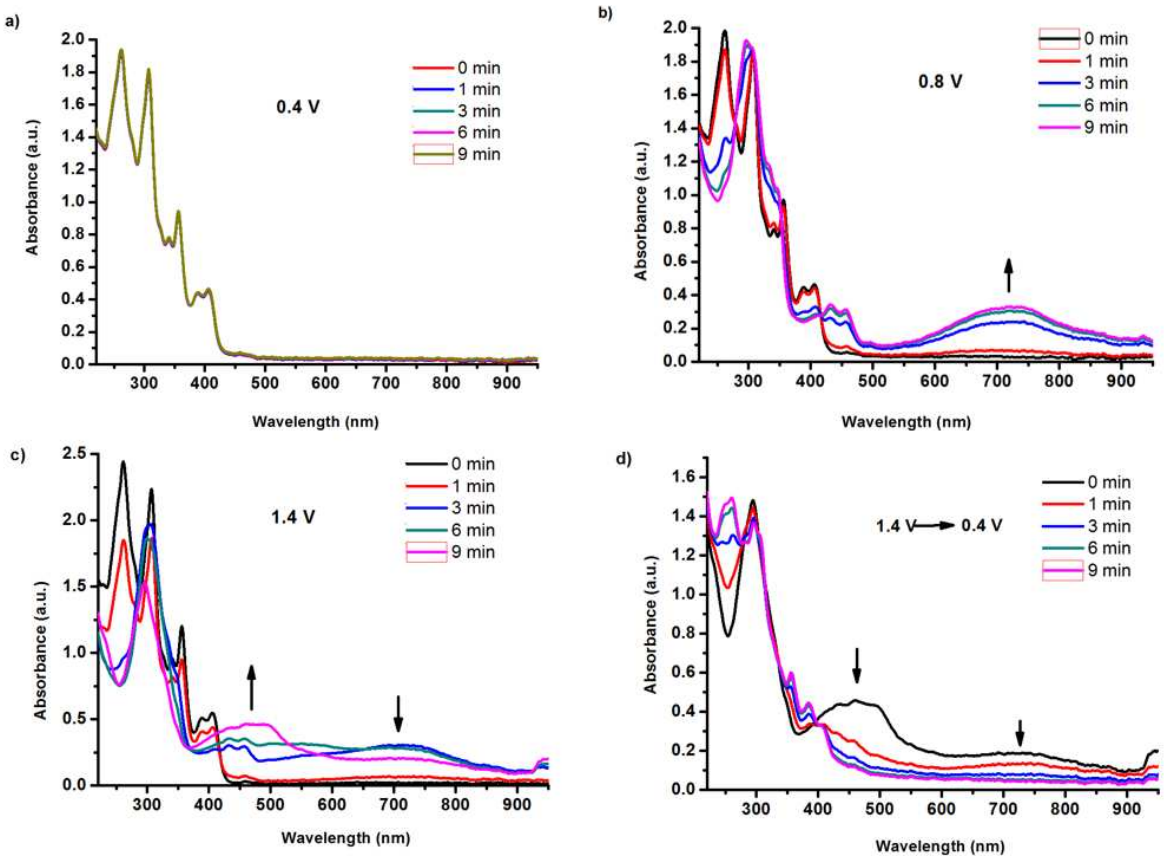

Figure S5: Spectroelectrochemistry of **2c** in acetonitrile solution containing 0.1 M Bu_4NPF_6 as supporting electrolyte at a) 0.4 V, b) 0.8 V c) 1.4 V and d) recovery of the compound from 1.4 to 0.4 V.

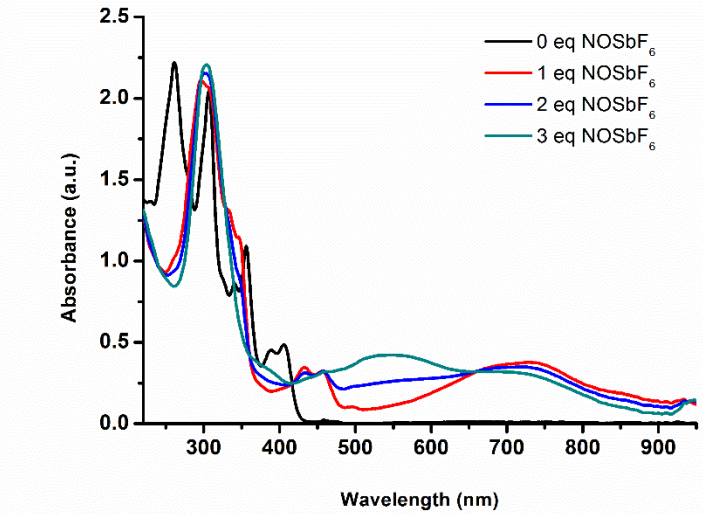

Figure S6 Chemical oxidation of **2c** in acetonitrile with different equivalent of $NOSbF_6$.

5. DFT calculations

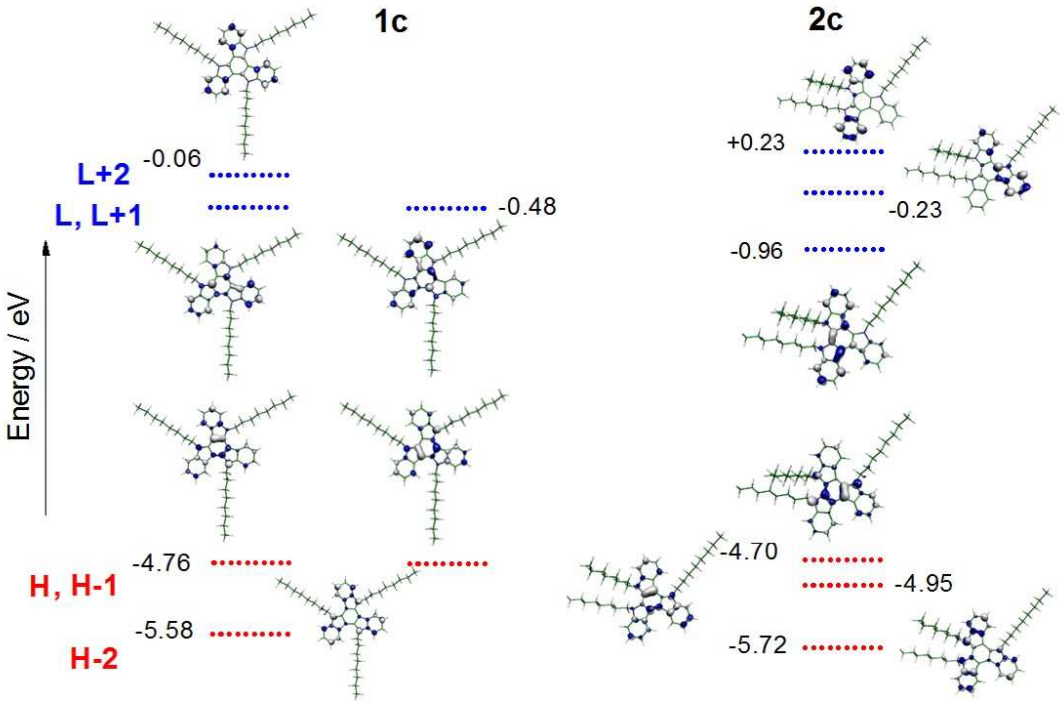

Figure S7. DFT//B3LYP/6-31G** molecular orbital energies and topologies for **1c** and **2c**.

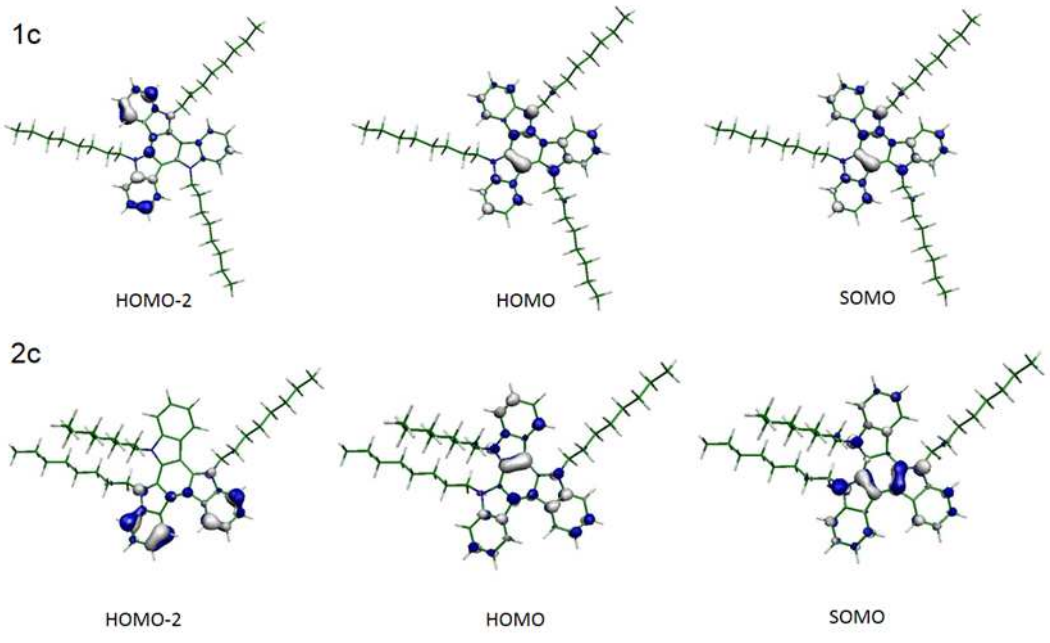

Figure S8. DFT// B3LYP/6-31G** molecular orbitals involved in the orbital transitions associated with the optical bands of radical cation species of **1c** (top) and **2c** (bottom).

Table S1. Vertical transition energies and oscillator strengths (f) calculated using TD-DFT//B3LYP/6-31G** for the **1b** and **2b** systems.

compound	TDDFT//B3LYP/6-31G**	
	Calculated Transition energy (eV)	**description**
1b	4.02 (f=0.45)	**H →L, H-1→L +1**
	4.02 (f=0.45)	**H-1 →L, H →L+1**
	4.23 (f=0.16)	**H →L+2**
	4.23 (f=0.16)	**H-2 →L+2**
	4.89 (f=0.30)	**H →L+5**
	4.89 (f=0.30)	**H-1 →L+5**
$1b^{\bullet+}$	1.11 (f=0.05)	**H-1 →S**
	1.83 (f=0.14)	**H-2 →S**
	3.96 (f=0.16)	**H-1→L, H-9→S**
$1b^{+}$	1.29 (f=0.09)	**H-1→L**
	1.76 (f=0.10)	**H-3→L, H-2→L**
	2.17 (f=0.29)	**H-2→L, H-3→L**
$2b^{+2}$	3.21 (f=0.13)	**H →L**
	3.56 (f=0.21)	**H-1→L**
	3.99 (f=0.10)	**H →L+1**
	4.19 (f=0.10)	**H-2 →L**
	4.29 (f=0.27)	**H-2 →L, H-1→L+1**
	4.34 (f=0.28)	**H →L+2**
	4.79 (f=0.16)	**H →L+4**
	4.93 (f=0.40)	**H →L+5**
$2b^{\bullet+}$	1.42 (f=0.06)	**H-1 →S**
	1.73 (f=0.10)	**H-2 →S**
	3.85 (f=0.22)	**H→L**
$2b^{+2}$	1.57 (f=0.15)	**H-1→L**
	2.00 (f=0.17)	**H-2→L**
	2.16 (f=0.08)	**H-4→L**
	2.65 (f=0.05)	**H-5→L**

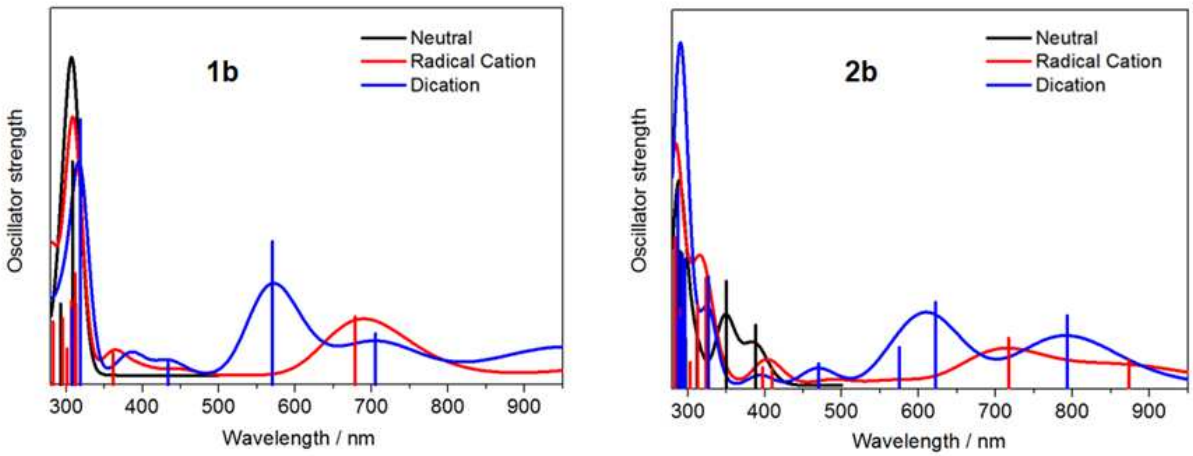

Figure S9. Simulated absorption spectra for **1b** (left) and **2b** (right) in the neutral, cation and dication states together with the TD-DFT//B3LYP/6-31G** excitations (wavelenght vs. oscillator strength) shown as vertical bars.

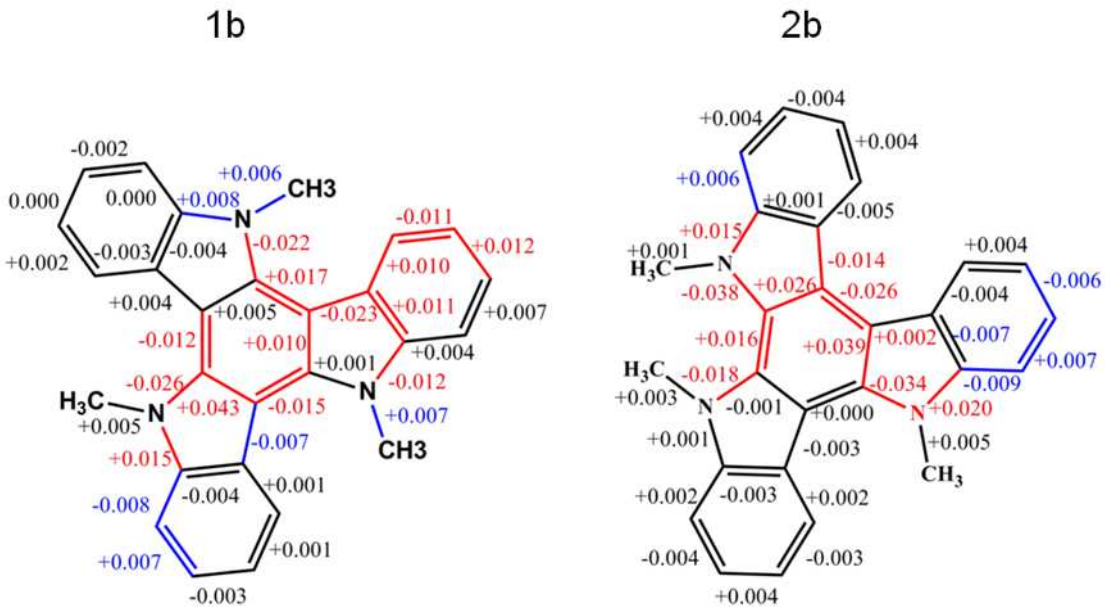

Figure S10. DFT-B3LYP/6-31G** calculated bond-length modifications (Å) for **1b** and **2b** molecules upon oxidation. The bond length modifications (Δx) larger than 0.010 Å are highlighted in red and those highlighted in blue corresponds to 0.005 Å <Δx > 0.010 Å.

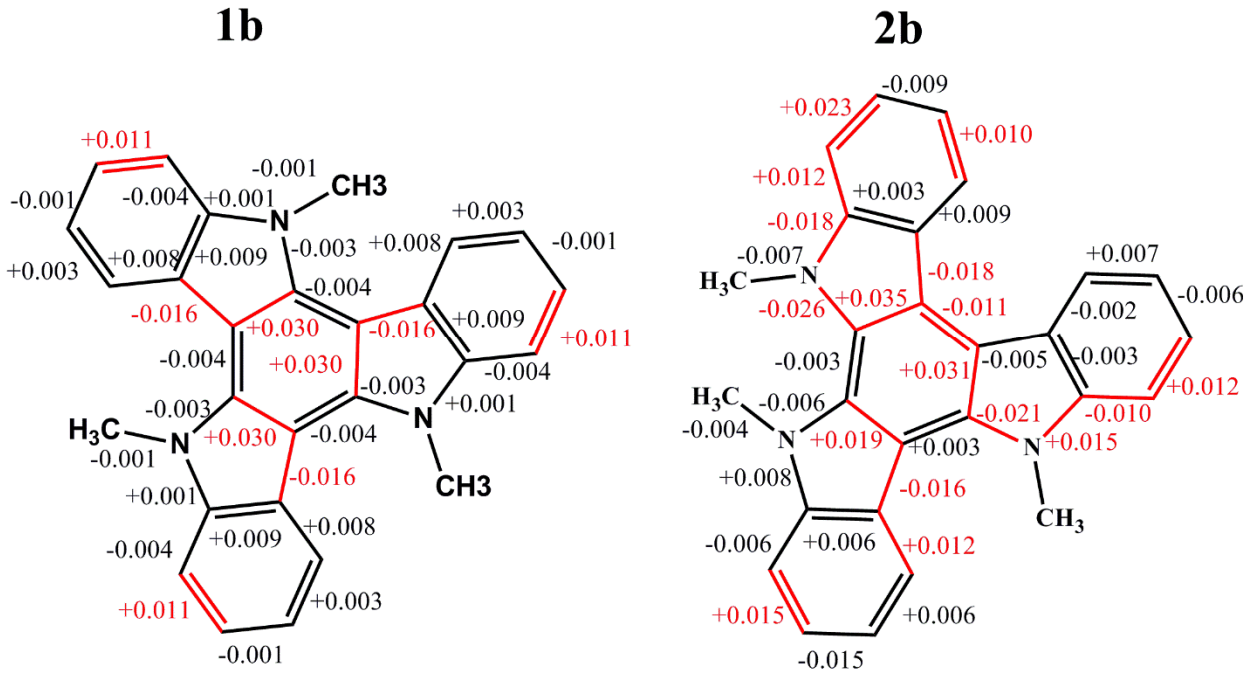

Figure S11. DFT-B3LYP/6-31G** calculated bond-length modifications (Å) for **1b** and **2b** molecules upon going from the S_0 ground state to the S_1 excited state. The bond length modifications (Δx) larger than 0.010 Å are highlighted in red.

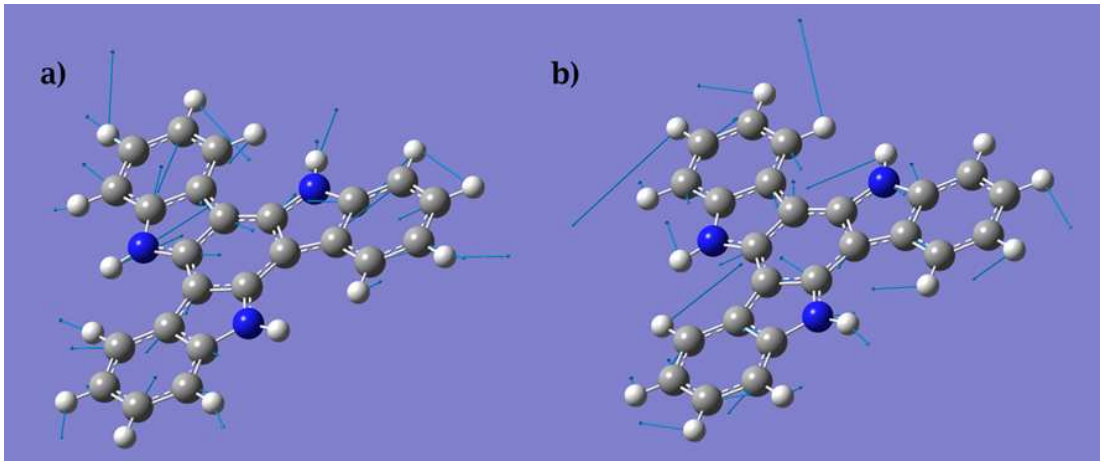

Figure S12. Representation of the **1a** 632 cm-1 (a) mode and 1330 cm-1 (b) S_1 modes presented on Table S3.

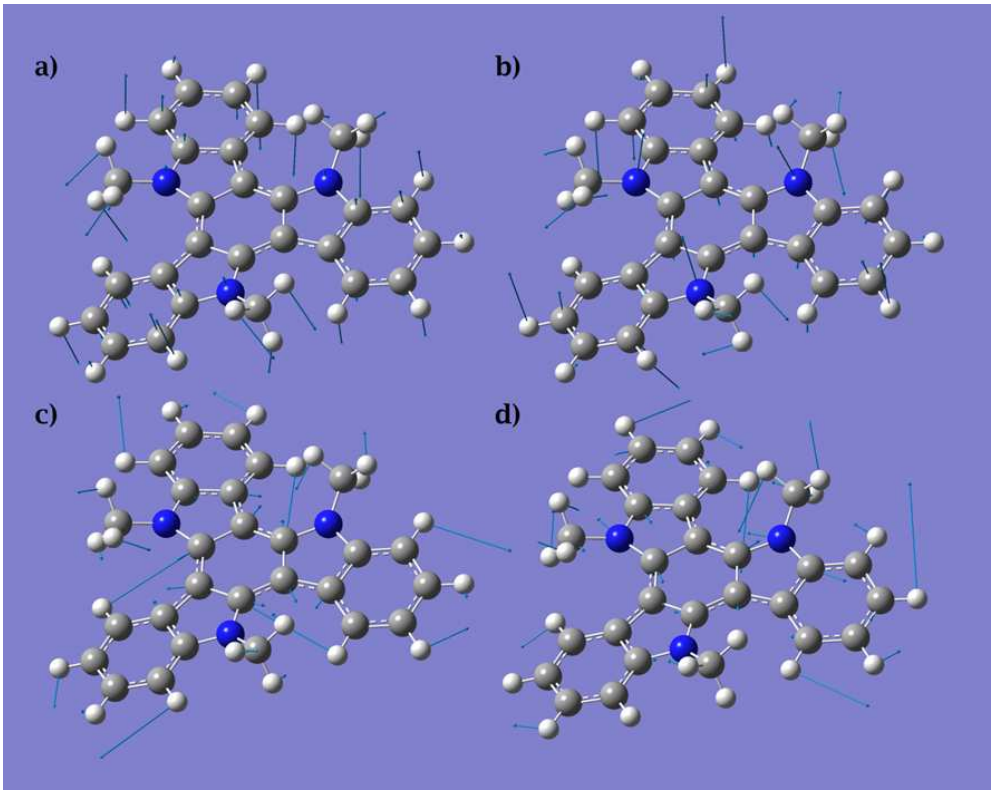

Figure S13. Representation of the **1b** 120 cm^{-1} (a), 333 cm^{-1} (b), 1243 cm^{-1} (c) and 1340 cm^{-1} (d) S_1 modes presented in table S4.

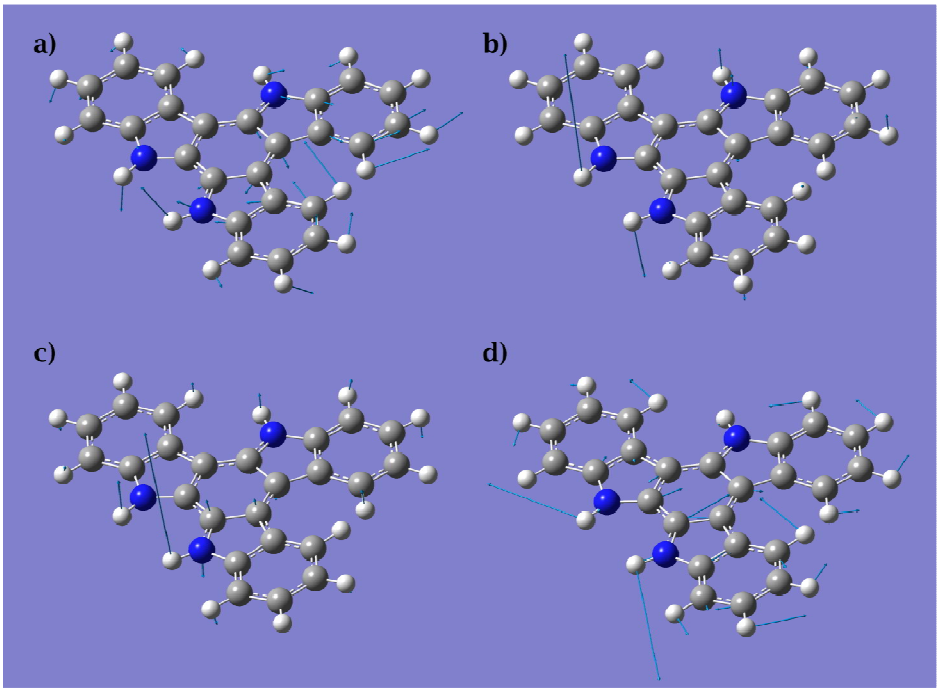

Figure S14. Representation of the **2a** 243 cm^{-1} (a), 293 cm^{-1} (b), 397 cm^{-1} (c) and 1329 cm^{-1} (d) S_1 modes presented in Table S5.

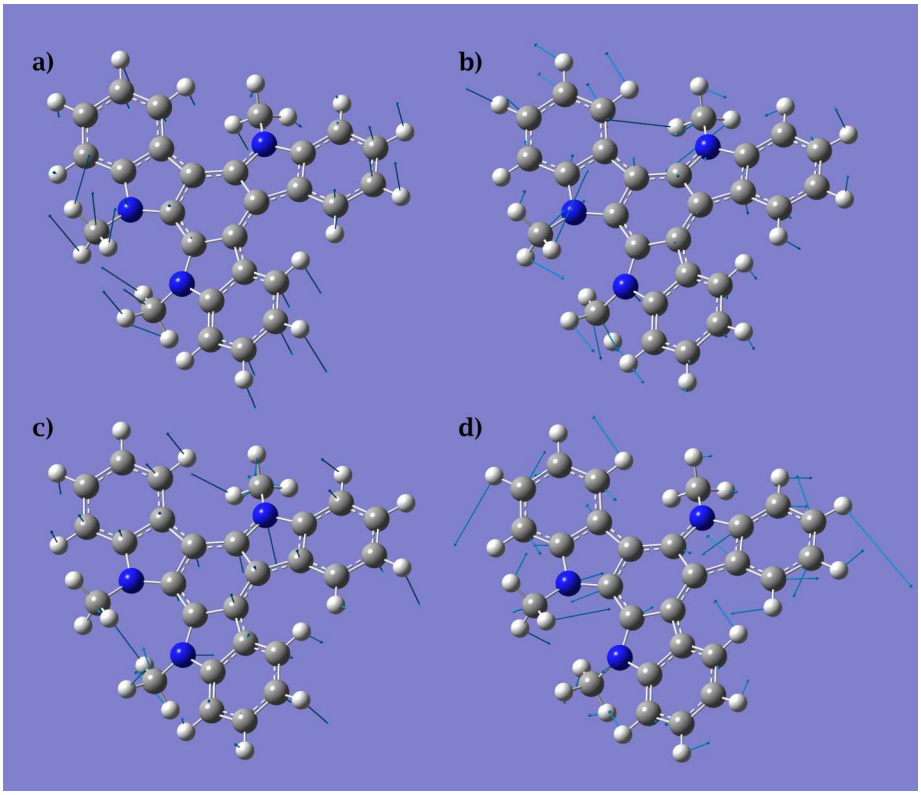

Figure S15. Representation of the **2b** 39 cm^{-1} (a), 262 cm^{-1} (b), 303 cm^{-1} (c) and 1394 cm^{-1} (d) S_1 modes presented in table S6.

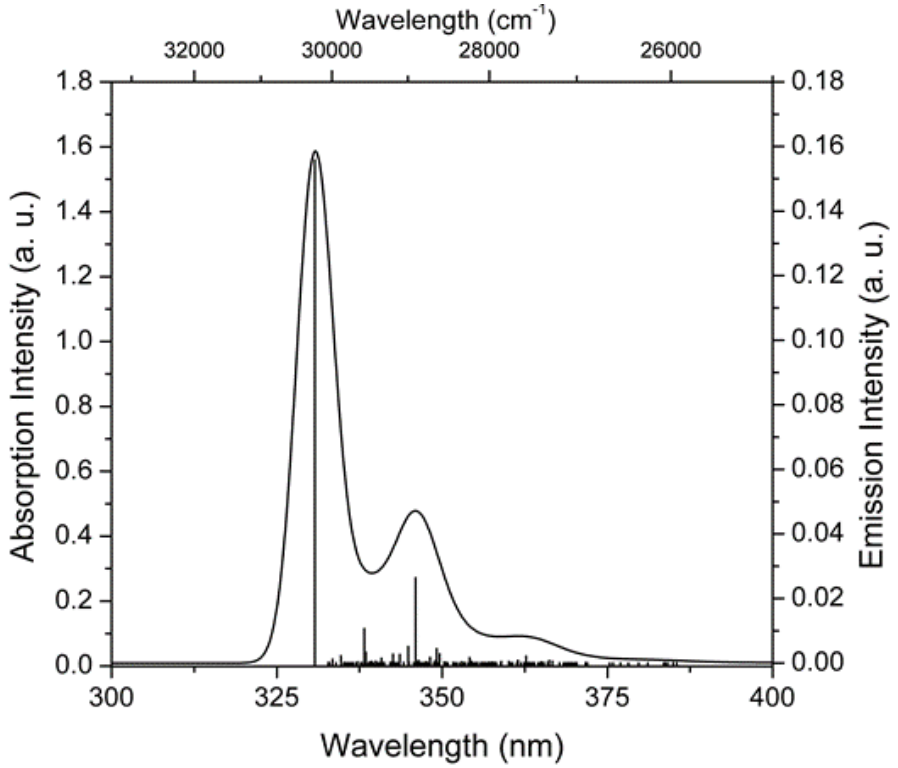

Figure S16. Emission ($S_1 \rightarrow S_0$) vibrational progression of **1a** together with the transitions with intensities larger than 1E-5.

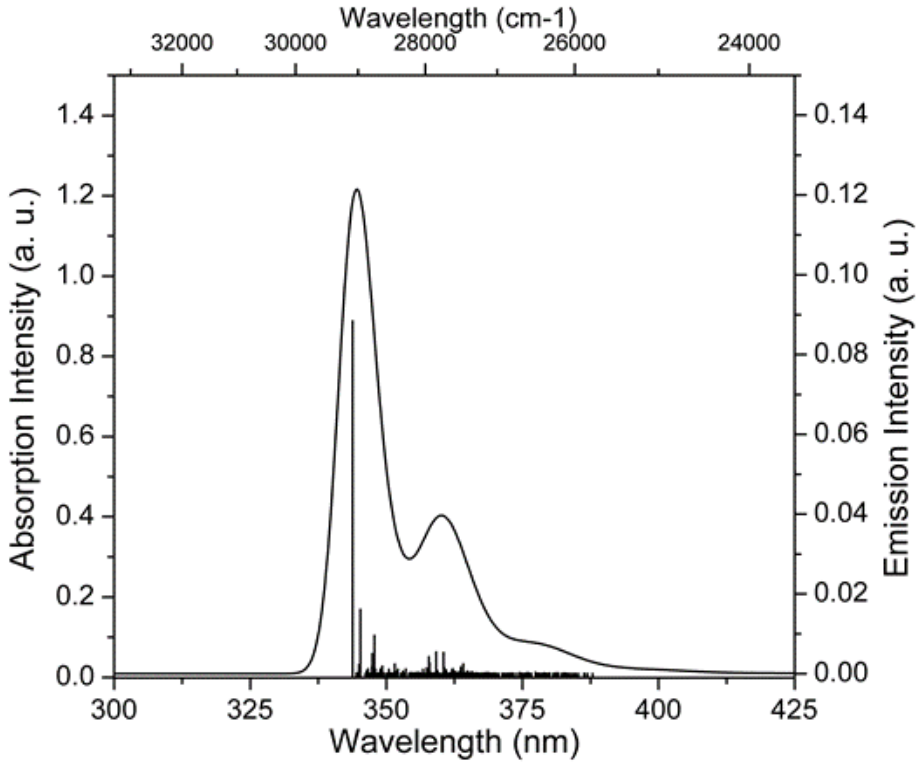

Figure S17. Emission ($S_1 \rightarrow S_0$) vibrational progression of **1b** together with the transitions with intensities larger than 1E-5.

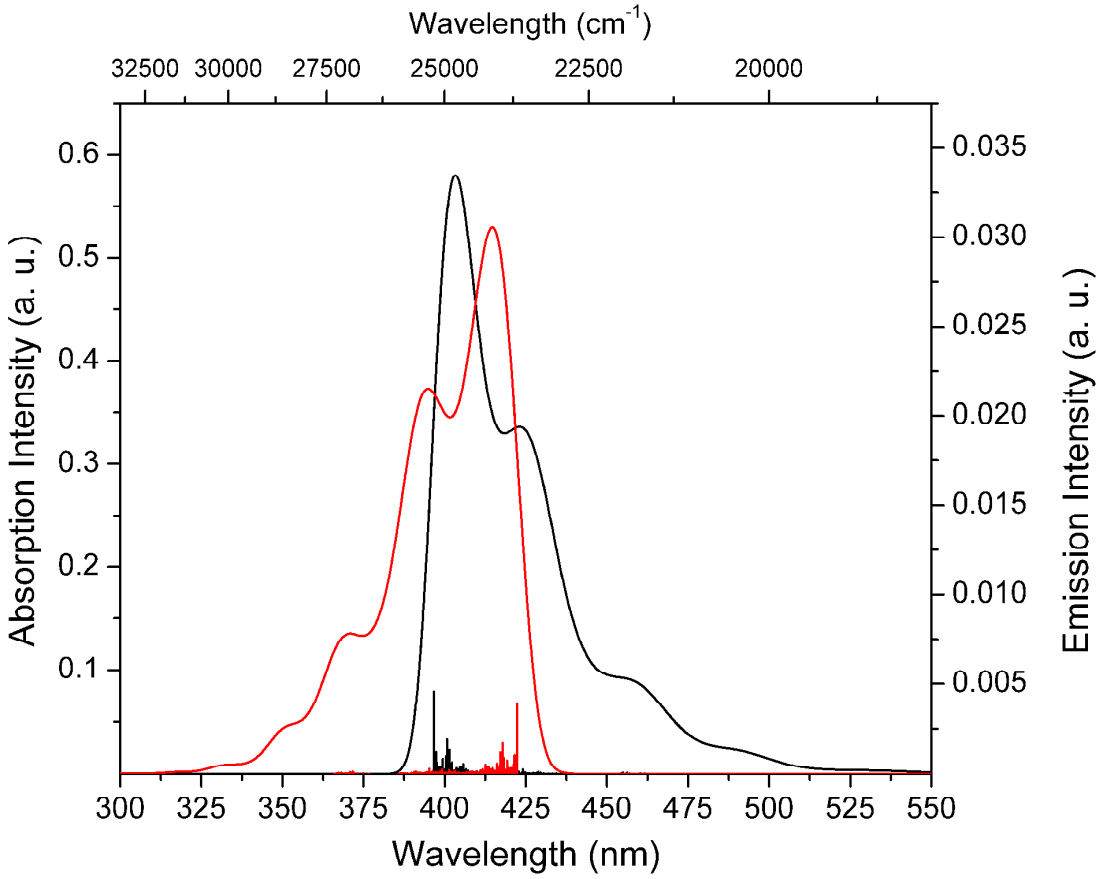

Figure S18. Absorption ($S_0 \rightarrow S_1$) (red) and emission ($S_1 \rightarrow S_0$) (black) vibrational progression of **2a** together with the transitions with intensities larger than 1E-5.

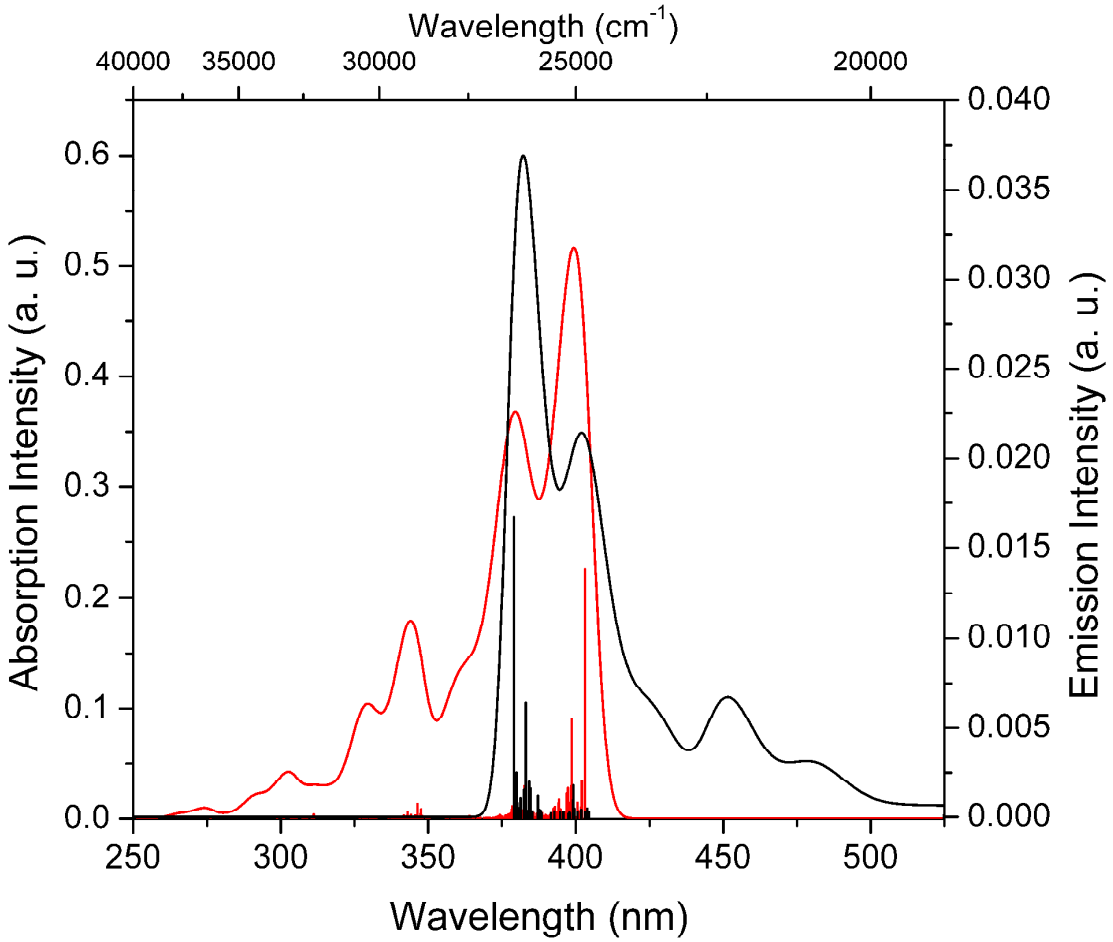

Figure S19. Absorption ($S_0 \rightarrow S_1$) (red) and emission ($S_1 \rightarrow S_0$) (black) vibrational progression of **2b** together with the transitions with intensities larger than 1E-5.

Table S2. $S_1 \rightarrow S_0$ relaxation energies computed by substracting the ground state energy at the S_1 geometry and the ground state energy at the optimized ground state geometry.

compound	**DFT//B3LYP/6-31G****
	$\lambda^{S_1 \rightarrow S_0}$ (meV)
1a	67
1b	80
2a	143
2b	177

Table S3. Frequency, S (Huang-Rhys) factor and corresponding relaxation energy for **1a** emission. Only modes with S larger than 0.1 are presented.

Frequency (cm^{-1})	S	λ (meV)
632	0.1	5
1330	0.2	34

Table S4. Frequency, S (Huang-Rhys) factor and corresponding relaxation energy for **1b** emission. Only modes with S larger than 0.1 are presented.

Frequency (cm^{-1})	S	λ (meV)
120	0.2	3
303	0.1	2
333	0.1	5
1149	0.1	10
1243	0.1	15
1340	0.1	12

Table S5. Frequency, S (Huang-Rhys) factor and corresponding relaxation energy for **2a** emission. Only modes with S larger than 0.1 are presented.

Frequency (cm^{-1})	S	λ (meV)
69	0.1	1
89	0.1	1
139	0.1	1
162	0.1	1
243	0.3	8
264	0.1	4
293	0.2	7
397	0.2	8
1259	0.1	11
1329	0.2	29
1392	0.1	9
3667	0.1	27

Table S6. Frequency, S (Huang-Rhys) factor and corresponding relaxation energy for **2b** emission. Only modes with S larger than 0.1 are presented.

Frequency (cm^{-1})	S	λ (meV)
39	0.3	2
50	0.2	1
64	0.2	2
102	0.2	2
116	0.1	2
176	0.1	1
262	0.5	17
303	0.2	7
354	0.1	3
362	0.2	9
1145	0.1	10
1250	0.1	8
1394	0.1	15
1648	0.1	14